

# Properties of HPK UFSD after neutron irradiation up to $6e15 \text{ n/cm}^2$

Z. Galloway, V. Fadeyev, P. Freeman, E. Gkougkousis<sup>2</sup>, B. Gruey, C.A. Labitan, Z. Luce,  
F. McKinney-Martinez, H. F.-W. Sadrozinski<sup>1</sup>, A. Seiden, E. Spencer, M. Wilder, N. Woods,  
A. Zatserklyaniy, Y. Zhao  
*SCIPP, Univ. of California Santa Cruz, CA 95064, USA*

R. Arcidiacono, N. Cartiglia, F. Cenna, M. Ferrero, R. Mulargia, A. Staiano, V. Sola  
*INFN, Torino, Italia*

V. Cindro, G. Kramberger, I. Mandić, M. Mikuž, M. Zavrtanik  
*Jožef Stefan institute and Department of Physics, University of Ljubljana, Ljubljana, Slovenia*

K. Yamamoto, S. Kamada, A. Ghassemi, K. Yamamura  
*Hamamatsu Photonics (HPK), Hamamatsu, Japan*

**Abstract**– In this paper we report results from a neutron irradiation campaign of Ultra-Fast Silicon Detectors (UFSD) with fluences of  $1e14$ ,  $3e14$ ,  $6e14$ ,  $1e15$ ,  $3e15$  and  $6e15 \text{ neq/cm}^2$ . The UFSD used in this study are circular  $50 \mu\text{m}$  thick Low-Gain Avalanche Detectors (LGAD), with a  $1.0 \text{ mm}$  diameter active area. They have been produced by Hamamatsu Photonics (HPK), Japan, with pre-radiation internal gain in the range 5-70 depending on the bias voltage. The sensors were tested pre-irradiation and post-irradiation with minimum ionizing particle (MIPs) from a  $^{90}\text{Sr}$  based  $\beta$ -source. The leakage current, internal gain and the timing resolution were measured as a function of bias voltage at  $-20^\circ\text{C}$  and  $-30^\circ\text{C}$ . The timing resolution was extracted from the time difference with a second calibrated UFSD in coincidence, using the constant fraction method for both. The dependence of the gain upon the irradiation fluence is consistent with the concept of acceptor removal; for this reason the gain decreases from about 80 pre-irradiation to 7 after a fluence of  $6e15 \text{ n/cm}^2$ . Consequently, the timing resolution was found to deteriorate from 20 ps to 50 ps. The results indicate that the most accurate time resolution is obtained at a value of the constant fraction discriminator (CFD) threshold used to determine the time of arrival varying with fluence, from  $\text{CFD} \approx 10\%$  pre-radiation to  $\text{CFD} \approx 60\%$  at the highest fluence. Key changes to the pulse shape induced by irradiation, i.e. (i) a reduced sensitivity of the pulse shape on the initial non-uniform charge deposition, (ii) the shortening of the rise time and (iii) the reduced pulse height, were compared with the WF2 simulation program and found to be in agreement.

PACS: 29.40.Gx, 29.40.Wk, 78.47jc

Keywords: fast silicon sensors; charge multiplication; thin tracking sensors; radiation damage; time resolution.

## 1 INTRODUCTION

We are developing a new type of silicon detector, the so-called ultra-fast silicon detector (UFSD) that would establish a new paradigm for space-time particle tracking [1]. The UFSD is a single device that ultimately will measure with high precision concurrently the space ( $\sim 10 \mu\text{m}$ ) and time ( $\sim 10 \text{ ps}$ ) coordinates of a particle.

UFSD are thin pixelated n-on-p silicon sensors based on the Low-Gain Avalanche Detector (LGAD) design [2] [3][4] developed by the Centro Nacional de Microelectrónica (CNM) Barcelona in part as a RD50 Common Project [5]. The sensor exhibits moderate internal gain ( $\sim 5$ -70) due to a highly doped  $p^+$  region just below the n-type implants. In [6] we have shown that a time resolution of below 35 ps can be achieved in a beam test with un-irradiated  $45 \mu\text{m}$  thick UFSD fabricated by CNM, adding for the first time timing resolution results on thin LGAD to the measurements on thicker sensors in beam tests and with laser laboratory measurements reported

---

<sup>1</sup> Corresponding author: hartmut@ucsc.edu, telephone (831) 459 4670, FAX (831) 459 5777

<sup>2</sup> Now at IFAE, Barcelona, Spain

before [7][8]. All these measurements at different sensors thicknesses agreed with the predictions of the simulation program Weightfield2 (WF2) [9].

First applications of UFSD are envisioned in upgrades of experiments at the High-Luminosity Large Hadron Collider (HL-LHC [10]) in ATLAS and CMS as reviewed in [11]. In all cases, the UFSD would be of moderate segmentation (a few  $\text{mm}^2$ ) with challenging radiation requirements (fluences up to several  $10^{15} \text{ neq/cm}^2$ ). Results on irradiated CNM LGAD 300  $\mu\text{m}$ , 75  $\mu\text{m}$  and 45  $\mu\text{m}$  thick sensors are presented in [12], [13], [14], where the timing resolution has been shown to deteriorate with fluence due to the loss in gain caused by the “acceptor removal mechanism” [15].

In this paper, we report on the results of the irradiation campaign of UFSD produced by Hamamatsu Photonics, Japan (HPK). In Section 2 we will describe the characteristics of the 50  $\mu\text{m}$  UFSD manufactured by HPK followed in Section 3 by a short description of the neutron irradiation. In Section 4 a description of the experimental set-up is presented, including the readout electronics and the laboratory  $^{90}\text{Sr}$   $\beta$ -source used for charge collection studies mentioned in [6]. In Section 5, we will describe the data analysis including the extraction of the gain, timing resolution and pulse characteristics while in Section 6 the results on bias dependence of leakage current, charge collection and gain, pulse characteristics, timing resolution for a range of neutron fluences, will be presented. Section 7 shows the comparison of results with predictions by WF2.

## 2 PRE-RADIATION PROPERTIES OF HPK UFSD

The UFSD were manufactured by HPK on 6” silicon wafers of 150  $\mu\text{m}$  total thickness with a 50  $\mu\text{m}$  or 80  $\mu\text{m}$  thick high resistivity float zone (FZ) active layer. HPK run #ECX20840 contains a variety of pad structures, with single pads of area  $\sim 0.8 \text{ mm}^2$  and 2x2 arrays of  $3 \times 3 \text{ mm}^2$  pads. The study presented in this paper used the 50  $\mu\text{m}$  thick single pads, which were produced in four “gain splits” (named “A” to “D”), identical in the mask design but with a different  $p^+$  dose of the gain layer, to study the optimum parameters of the charge multiplication mechanism. The C-V measurements indicate that the difference between doping concentrations of adjacent splits is about 4% [16]. The leakage currents are very low before breakdown, less than 100 pA.

The gain was measured using the read-out board described in Section 3 and  $\beta$ -particles from the  $^{90}\text{Sr}$  source. As shown later, the gain is computed by comparing the collected charge to the charge expected from a MIP in an equivalent sensor without gain. Using Ref. [17] this is estimated to be 0.51 fC for un-irradiated sensors, while it was calculated for every neutron fluence used with the simulation program WF2 [9].

Figure 1 shows the gain as a function of bias voltage for 50  $\mu\text{m}$  thick single pads from the four splits A-D, and for two pads of 80  $\mu\text{m}$  thickness for splits B and D. Figure 1 shows that the split D has the highest doping initial concentration, and split A the lowest. For the 80  $\mu\text{m}$  thick sensors, splits A and B have a gain much lower than 10 when biased below 800V.

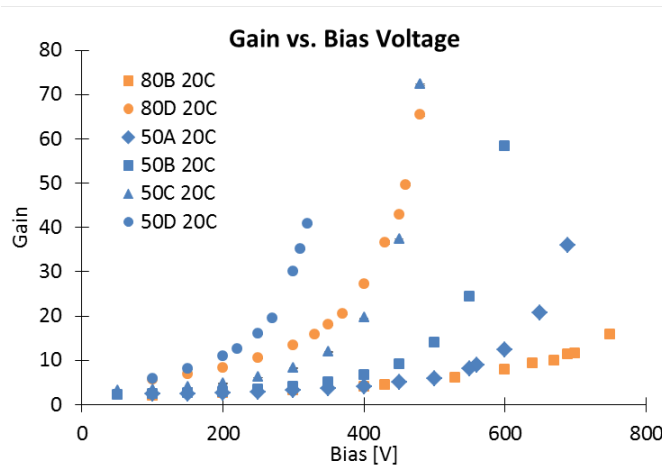


Fig. 1: Gain vs. Bias voltage for the HPK 50  $\mu\text{m}$  and 80  $\mu\text{m}$  thick LGAD at +20°C. The four different sensors A-D reflect the four different doping profiles of the multiplication layer [18].

The results presented in the following are obtained using thin 50  $\mu\text{m}$  LGAD only, mostly with the highest gain implant dose, “D”, and one LGAD with “C” for comparison. Sensors with the highest doping concentration were chosen because irradiated CNM LGAD showed that sensors with higher initial doping concentration retained after irradiation higher acceptor concentration than those with lower initial concentration [12] [13] [14]. In Section 6.1, this fact is shown to apply to HPK sensors too.

### 3 NEUTRON IRRADIATION

The LGAD were irradiated without bias in the Ljubljana TRIGA reactor which has been used successfully in the past years to support sensor development [19]. The neutron spectrum and flux are well known and the fluence is quoted in 1 MeV equivalent neutrons per  $\text{cm}^2$  ( $\text{neq}/\text{cm}^2$  or shortened  $\text{n}/\text{cm}^2$ ). After irradiation, the devices were annealed for 80 min at 60C. Afterward the devices were kept in -20C degree storage.

### 4 EXPERIMENTAL SET-UP

#### *Detector Readout*

For charge collection studies the UFSD are mounted on a  $10 \times 10 \text{ cm}^2$  read-out board developed at the University of California Santa Cruz (UCSC). It has been used in previous beam tests and is described in detail in [6]. The high bandwidth of more than 3 GHz allows the recording of the pulse shape of the fast LGAD signals by a 2.5 GHz – 8 bit vertical resolution LeCroy WavePro 725Zi-A digital oscilloscope at a sampling rate of 40 GS/s, therefore with a time discretization of 25 ps. This first inverting amplifier together with the following external commercial 20dB amplifier has a trans-impedance of  $4700 \Omega$ . An important part is the use of thin metal lids on both sides of the board to suppress pick-up. The scope noise contributes a varying fraction to the overall noise depending on the vertical scale used, and special care had to be taken to minimize that contribution. The effect is minimized by the fact that a large vertical scale (which has large scope noise) is used for large gain signals, at which point the jitter contribution is small (see Sec. 5 below).

#### *$^{90}\text{Sr}$ $\beta$ -Telescope*

The laboratory setup with  $^{90}\text{Sr}$   $\beta$ -source is shown in Fig. 2. A frame aligning the source, the device under test (DUT) and the trigger counter is placed in a climatic chamber. To allow passage of electrons through the DUT board, it has a hole centered on the LGAD, limiting the exposed area of the sensor. Because of the large radiation-induced leakage current, the irradiated LGAD were operated at -20C and -30C. The climatic chamber provides shielding against pick-up. The trigger and time reference is provided by a CNM LGAD which has a time resolution of 35 ps at +20C, measured in beam test [6], and of 27 ps at -20C as measured with a pair of identical LGAD.

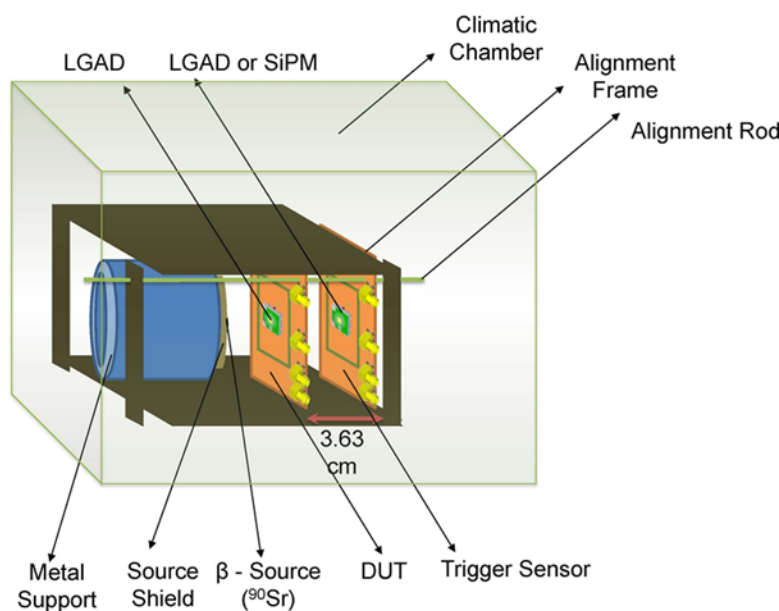


Fig. 2: The laboratory setup of the  $\beta$ -telescope consisting of alignment frame,  $^{90}\text{Sr}$ -source, the DUT LGAD and the trigger LGAD all housed in a climatic chamber [20].

The very low noise level of the trigger LGAD allowed triggering at about 7 times its noise RMS. Following a trigger, the traces of both trigger and DUT were recorded, with a rate of a few Hz. About 30% of the triggers consist of good signal coincidences between DUT and trigger LGAD.

## 5 DATA ANALYSIS

The analysis follows the steps listed in [6]; additional details of the analysis can be found in [20]. The digital oscilloscope records the full waveform of both trigger and DUT in each event, so the complete event information is available for offline analysis. Average and normalized pulses for three different fluences are shown in Figs. 10 and 15 below.

The main difference to previous measurements is the use of a variable threshold of the constant fraction discriminator (CFD) which defines the time of arrival of a particle as the time at which the signal crosses a certain fraction of the maximum signal amplitude, and it is an efficient tool to correct for the time walk (cf. eq (2) below). Adjusting the CFD threshold for every bias voltage and fluence allows optimizing the time resolution.

The event selection is straightforward: for a valid trigger pulse, the signal amplitude  $P_{\text{max}}$  of the DUT UFSD should not be saturated by either the scope or the read-out chain. To eliminate the contributions from non-gain events or noise, the time  $T_{\text{max}}$  of the pulse maximum has to fall into a window of 1 ns centered on the CFD threshold of 20% of the trigger. Figure 3 shows the distribution of the time of the 20% CFD level of the DUT (correcting for the trigger time walk by subtracting the time of the 20% CFD of the trigger), indicating very little noise. The distribution is dominated by the gain events, but a small fraction of no-gain events are seen at early times, possibly due to a small misalignment of the DUT with respect to the hole in the board.

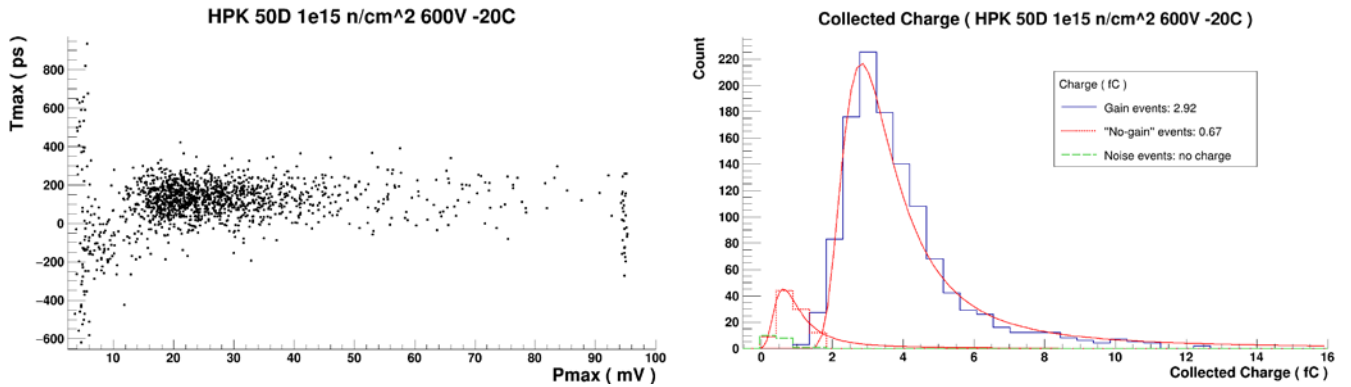


Fig. 3: Scatter plot of the time of the pulse maximum  $T_{\text{max}}$  vs. the maximum pulse height  $P_{\text{max}}$  for the LGAD (left) exposed to a neutron fluence of  $1\text{e}15\text{ n/cm}^2$ . The collected charge with time close to the trigger time show the form of a Landau distribution (right).

The gain is measured by integrating the voltage pulse and dividing it by the trans-impedance of the amplifier. The collected charge distribution is then fit to a Landau curve and the MPV is divided by the MPV of the collected charge of a no-gain silicon detector with the same thickness and neutron fluence. It is important to note that even in 50 micron thick sensors the charge collected in a no-gain sensor is reduced by irradiation. Figure 4 shows the collected charge of a no-gain 50  $\mu\text{m}$  sensor as a function of neutron fluence in units of a non-irradiated sensor, according to WF2 simulations. After a fluence of  $6\text{e}15\text{ n/cm}^2$ , 50.5% of the charge of a pre-radiation sensor is still collected. The gain calculation has been verified with different signal sources ( $\beta$ -particles, laser, minimum ionizing particles with slow amplifiers) and electronics (integrating and fast read-out), and has an estimated common systematic scale error of 20%.

The time of arrival at a specific CFD fraction value was extracted from the recorded samples by means of a linear interpolation between the point above and below the requested value. By measuring the timing resolution as a function of the CFD fraction, a value for the CFD threshold which minimized the resolution was found. An analysis of the resolution as a function of separate CFD thresholds for each fluence yields an optimum CFD value for each fluence, affording an improved timing resolution.

The time resolution is derived from the sigma  $\sigma_{\Delta t}$  of a Gaussian fit to the time difference  $\Delta t$  between the DUT and the trigger, both corrected for time walk with its proper CFD level, and the resolution  $\sigma_t$  of the DUT is then calculated according to

$$\sigma_t = \sqrt{\sigma_{\Delta t}^2 - \sigma_{trig}^2}, \quad (1)$$

with the resolution of the trigger being  $\sigma_{trig} = 29$  ps at -20C and 27 ps at -30C.

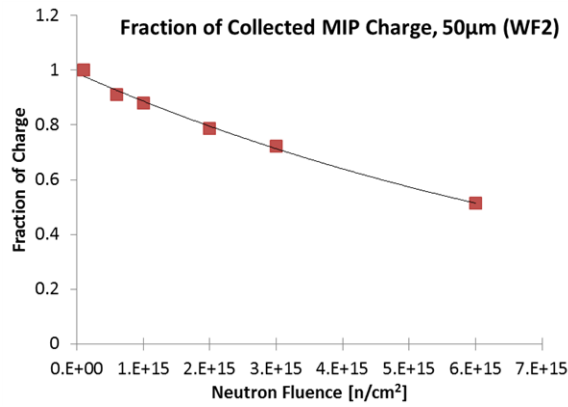


Fig. 4: Fraction of the collected charge of a MIP in a no-gain 50  $\mu\text{m}$  thick silicon detector as a function of neutron fluence relative to the pre-radiation collected charge of 0.51 fC, calculated using the WF2 program.

## 6 RESULTS OF BIAS SCANS

### 6.1 Gain

The UFSD gain as a function of bias for different neutron fluences are shown in Fig. 5 for operating temperatures of -20C and -30C. The bias required to reach a certain gain value increases with increased fluence due to the “acceptor removal” mechanism [15]: as the gain layer becomes less doped and generates a weaker electric field, the external bias voltage needs to be increased to compensate for this loss. The highest bias voltage which can be reached before the sensor exhibits instabilities is called the “breakdown voltage  $V_{BD}$ ” and will be discussed in Section 6.7. For the LGAD 50D the gain at  $V_{BD}$  is below 20 at fluences beyond  $6 \times 10^{14} \text{ n/cm}^2$  and below 10 beyond  $3 \times 10^{15} \text{ n/cm}^2$ . The sensor 50C reaches  $V_{BD} > 700\text{V}$  at  $6 \times 10^{14} \text{ n/cm}^2$  and gain  $< 20$ , similar to the sensor 50D at  $1 \times 10^{15} \text{ n/cm}^2$ , indicating the advantage of higher initial doping concentration mentioned in Section 2.

The simulations program Weightfield 2 [9] incorporates the parametrization of the measured acceptor removal [15] and predicts that when a bias value of about 600 – 650 V is reached, the electric field in the bulk becomes high enough to generate multiplication also in the sensor bulk, moving the location of the multiplication mechanism from the gain layer into the bulk.

For highly irradiated UFSD at fluences of  $1 \times 10^{15} \text{ n/cm}^2$  and  $6 \times 10^{15} \text{ n/cm}^2$  the bias voltage dependence of the gain is the same for -20C and -30C.

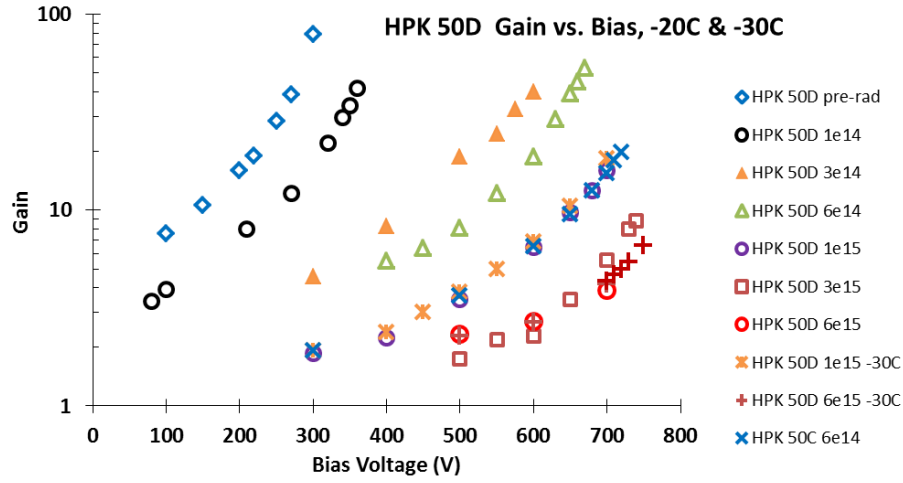


Fig. 5: Gain as a function of bias of the LGAD irradiated to the indicated neutron fluences at -20C and -30C, showing the need for increasing the bias of irradiated sensors to reach adequate gain. The gain has a common systematic scale error of 20%.

## 6.2 Leakage current

Like for no-gain silicon sensors, the leakage current of LGADs depends linearly on fluence and exponentially on the temperature (about factor 2 increase for every 7C degree increase). For LGADs, in addition, the current depends linearly on the gain. The leakage currents for the different fluences as a function of bias shown in Fig. 6 (left). The leakage currents with the same fluence but at different temperatures (-20C and -30C) show the expected ratio.

The leakage currents at the same fluence exhibit large increases for increased bias partially due to the increased gain. When dividing the current by the gain, as shown on Fig. 6 (right), the currents become much more leveled and the fluence dependence is recognized directly. The straight lines in Fig. 6 (right) are predictions of the leakage currents of no-gain sensors for the fluence indicated. The fact that the prediction are somewhat higher than the gain can be taken as an indication that part of the collected current does not undergo multiplication. This assumption is under investigation. The highest bias voltage reached for each fluence is close to the breakdown voltage  $V_{BD}$ , characterized by base line shifts and spurious breakdown pulses.

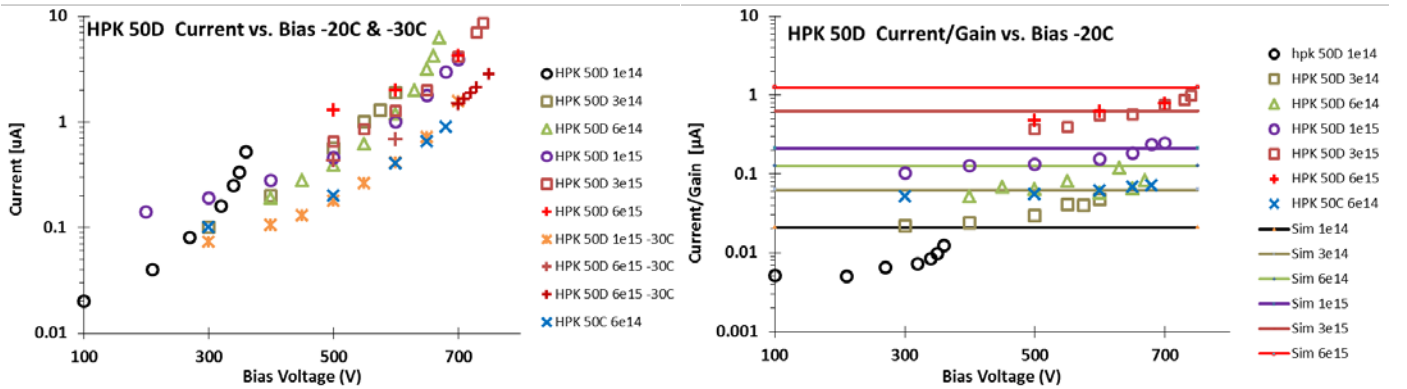


Fig. 6: Leakage current at -20C and -30C as a function of bias of the LGAD irradiated to the neutron fluences indicated (left), and the same data for -20C divided by the gain (right). The predicted currents for no-gain sensors for the fluences indicated are shown as horizontal lines.



### 6.3 Timing resolution

As Fig. 10 below shows, the pulse shape changes as a function of fluence. Thus we should anticipate the possibility that a fixed CFD fraction does not minimize the time resolution for all fluences (and even different gains). The CFD threshold scans in Fig.7 demonstrate that as a function of neutron fluence and bias voltage the time resolution is minimized at different values of the CFD fractions. (The legend denotes the values for bias voltage, fluence, temperature and gain). In Fig. 8 the CFD scans for several bias voltages for all fluences are shown, demonstrating a change in the curves above a fluence of  $1e15$  n/cm<sup>2</sup>. A comparison between the CFD scans at -20C and -30C for the  $6e15$  n/cm<sup>2</sup> data shows a 10% improvement of the timing resolution with a temperature decrease of 10C.

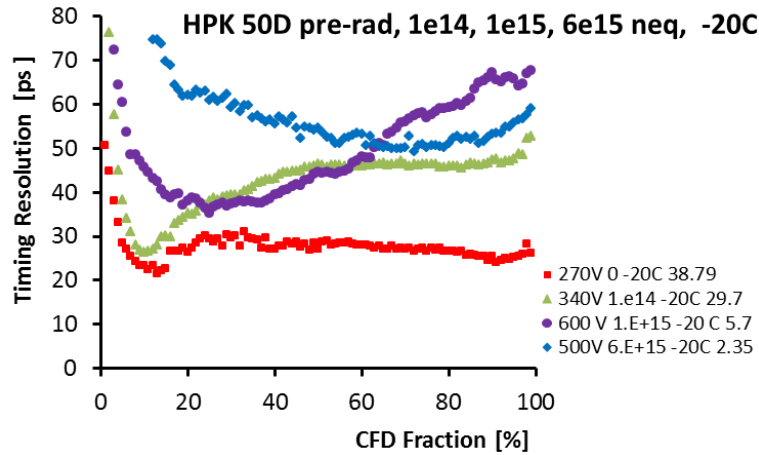
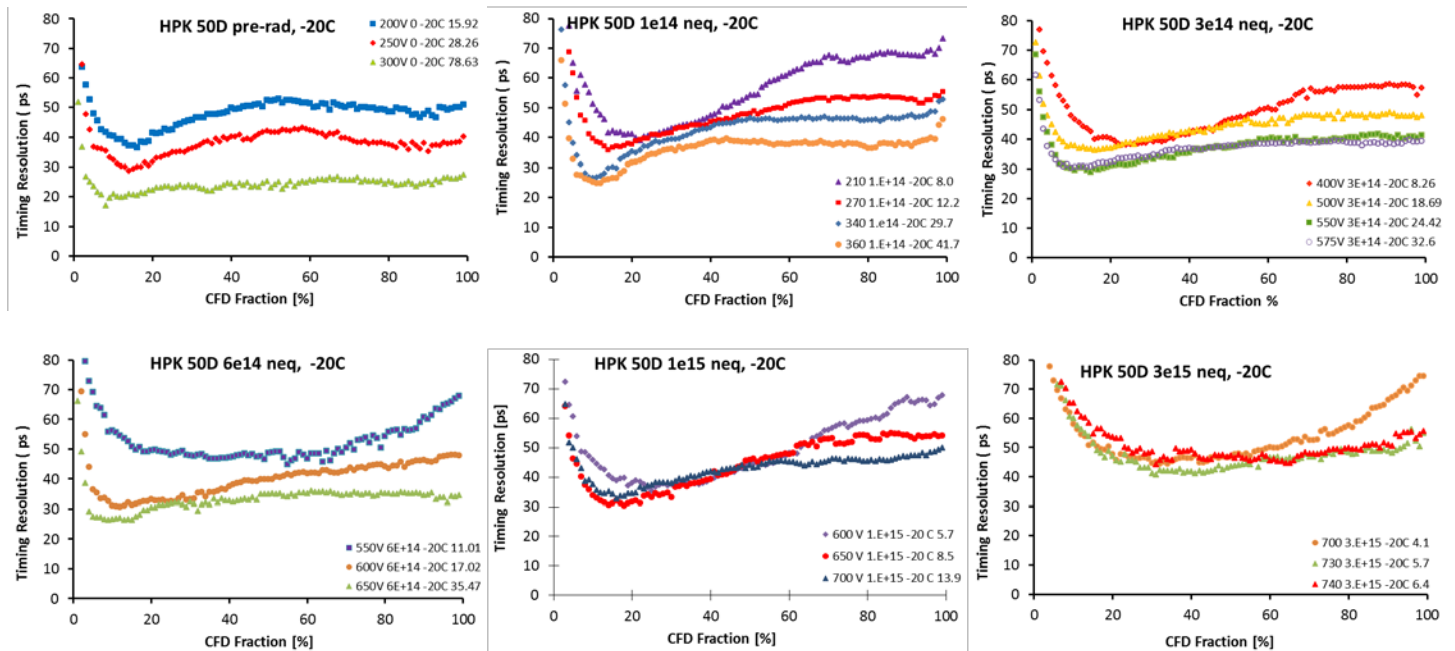


Fig. 7 Time resolution for selected fluences as a function of CFD threshold at VHR bias voltages defined below. The legends here and in the following are bias voltage, fluence, temperature, gain.



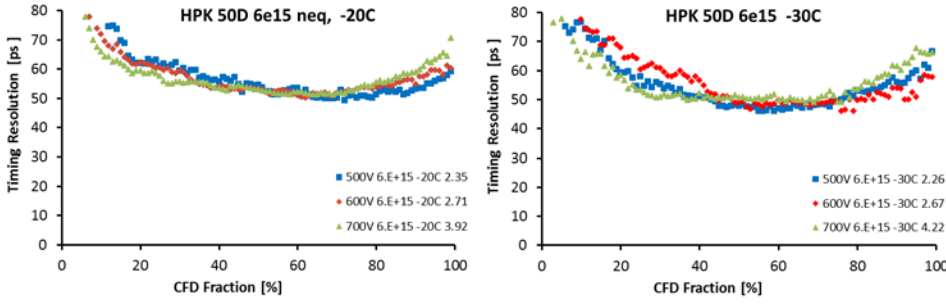


Fig. 8 CFD fraction scans for several bias voltages for each of the seven neutron fluences. Data were taken at -20C, with the exception of the last panel (6e15 n/cm<sup>2</sup>) at -30C which shows that the time resolution improves by 5ps when lowering the temperature by 10C.

Following [1], the timing resolution  $\sigma_t$  can be parametrized as

$$\sigma_t^2 = \sigma_{Jitter}^2 + \sigma_{LandauNoise}^2 + \sigma_{Distortion}^2 + \sigma_{Timewalk}^2 + \sigma_{TDC}^2 \quad , \quad (2)$$

and the main terms contributing are (i) the jitter,

$$\sigma_{Jitter} = \frac{N}{dV/dt} \approx \frac{t_{rise}}{\frac{S}{N}} \sim t_{rise} \frac{N}{G} \quad , \quad (3)$$

depending on the noise  $N$ , the rise time  $t_{rise}$  and the inverse of the gain, and (ii) the Landau noise, caused by the fluctuations of the ionization profile. As mentioned in Sec. 5, use of the CFD method minimizes the time walk and a “parallel plate” geometry minimizes distortion. As Fig. 9 shows, the time resolution is indeed falling with increasing gain. In the plot it is possible to identify at low gain two different groups, with the first one formed by the lower-fluence data up to 6e14 n/cm<sup>2</sup> and the second by higher-fluence data. For a fixed value of gain, for example gain = 5, the lower-fluence group has a worse time resolution than the higher-fluence group. This fact, which might seem counter-intuitive, is due to the different type of multiplication mechanism in the two groups: as mentioned in Section 6.1: below a fluence of 1e15 n/cm<sup>2</sup> the multiplication occurs mainly in the gain layer, while for the higher fluence sample the multiplication happens everywhere in the bulk, allowing for a much smoother process. The observed decrease of the rise time at higher fluence contributes to the improved time resolution (see below).

For the higher-fluence group the resolution worsens at the highest gains achieved, which in most cases can't be explained simply by the modest noise increase associated with higher gain. Thus the highest bias before breakdown,  $V_{BD}$ , is not necessarily the bias at which the best time resolution is reached.

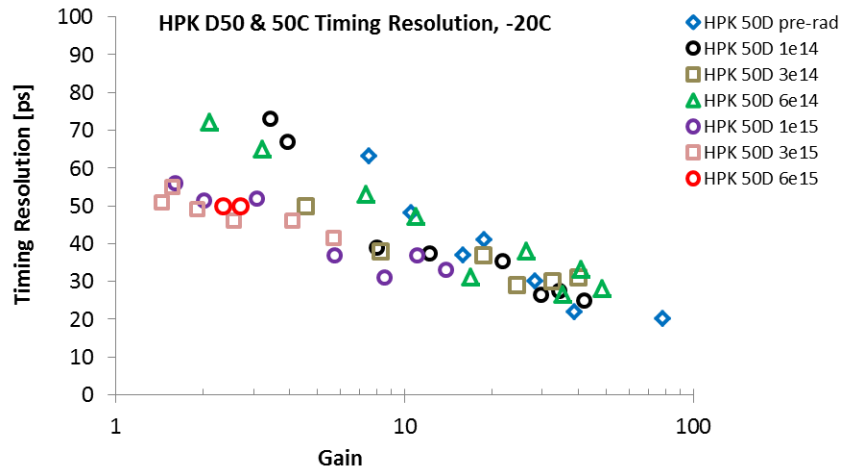




Fig. 9: Time resolution evaluated at an optimized CFD fractions vs. gain for the different fluences at -20C.

### 6.5 Rise Time

As shown above, the jitter depends on the gain and the rise time (c.f. Eq. (3)). At the same time Figs 9 indicates that the time resolution is not always optimized at the bias with the highest gain, and good time resolution for heavily irradiated LGAD is achieved at fairly low gain. A look at the average pulse for different fluences (Fig. 10) shows that the pulses change shape when the gain in the multiplication layer is reduced and the trapping is severe. The pre-radiation pulse is dominated by a “plateau top” due to the gain holes, while at  $6e15 \text{ n/cm}^2$  (i) the direct electrons and the gain electrons make the pulse front steeper and (ii) trapping reduces the pulse tail. Figure 11 shows the 10% - 90% rise time as a function of gain for the different fluences. We observe shorter rise times at small gain, when the gain layer makes only a small contribution, and they increase when the gain is increased. For larger gain (at low fluences) the rise time becomes as long as the electron drift time [1].

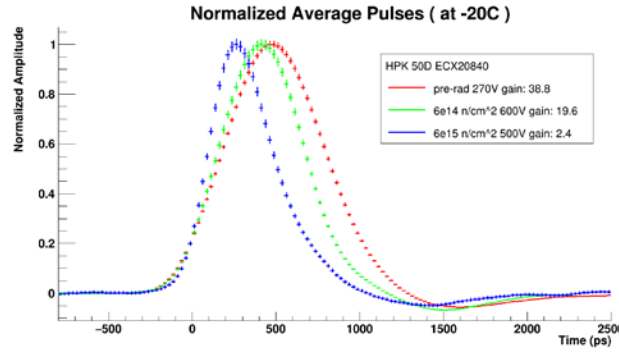


Fig. 10: Averaged pulse shapes at three bias voltages pre-radiation, and after fluences of  $6e14$  and  $6e15 \text{ n/cm}^2$ .

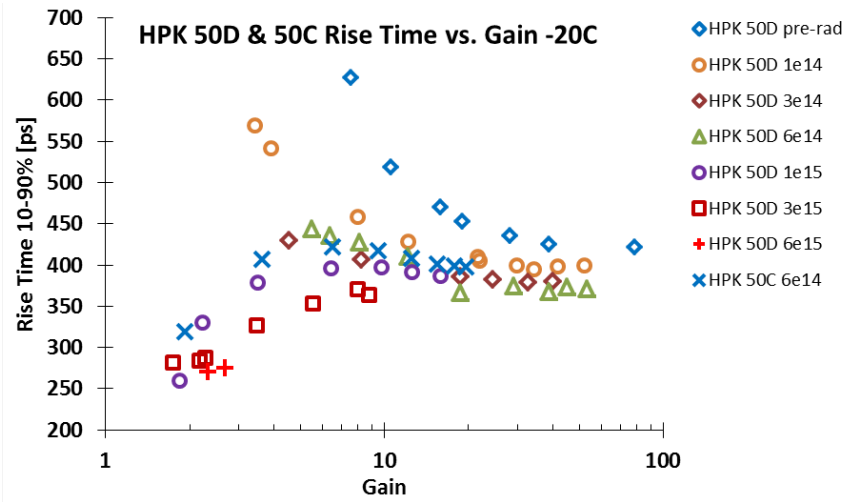


Fig. 11: Rise time 10% to 90% vs. gain for the different fluences and temperatures. Note (i) the low rise time at small gain, which increases when the gain is increased and (ii) for larger gain a decrease or saturation of the rise time one would expect from the saturation of the drift velocity with the bias voltage.

### 6.6 Jitter and Landau Fluctuation

In Section 6.3 we show a dramatic change in the fluence dependence of the time resolution on the value of the CFD fraction (cf. Fig. 8). This can be explained by the effect of the changing gain on both the Landau fluctuation and the jitter, which contribute to the time resolution (eq. 2).

The jitter extracted from the data using eq. (3),  $\sigma_{\text{jitter}} = N/(dV/dt)$ , is shown in Fig. 12. Here the slope  $dV/dt$  (Fig. 12, left) is calculated in a fit to the pulse shape using  $\pm 2$  neighboring time bins. The slope is maximized for all fluences with a CFD setting  $> 50\%$ . This means that the jitter (Fig. 12, right) is lowest for the CFD set at  $\sim 50\%$ . For those settings, the jitter depends largely on the gain which can be reached at the different fluences.

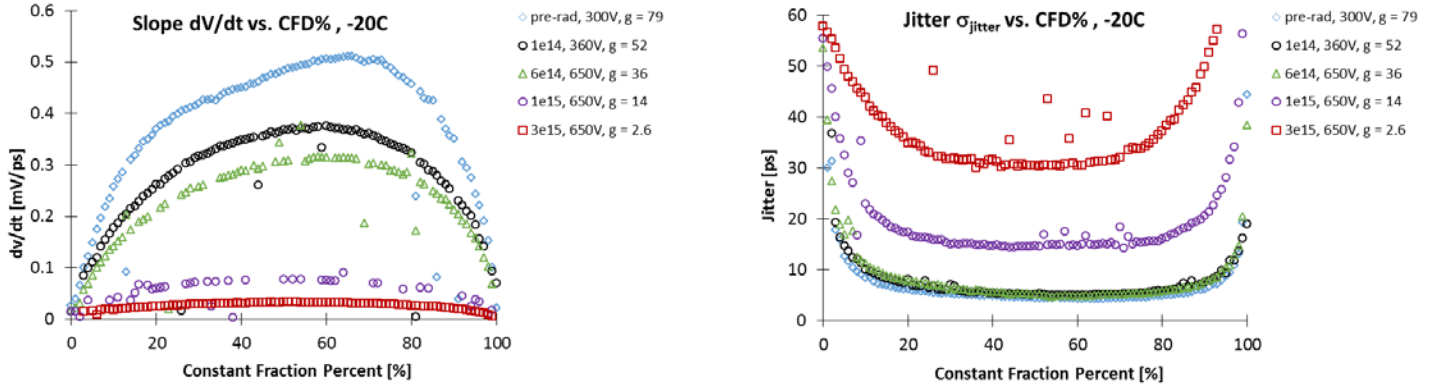


Fig. 12: Measured slope (left) and jitter (right) as a function of CFD fraction for several fluences. For low fluences and high gain, the contribution of the pre-jitter is small. For high fluences (low gain) it increases and determines the time resolution.

Figure 13 shows the prediction of WF2 for the Landau fluctuation for different fluences as a function of gain: pre-radiation with high gain (Fig. 13, left) the contribution is minimized with a low CFD setting for all thicknesses; as a function of gain (Fig. 13, right) at low CFD setting for all fluences (and even for no-gain sensors) WF2 predicts the contribution of the Landau fluctuations to be small for low gain. The circle indicates that for values of  $\sim 5$  the contribution is roughly constant with irradiation.

The relative size of jitter and Landau fluctuations determines the optimal CFD setting: for low fluences (high gain) the jitter is low and the larger Landau fluctuations are minimized at low CFD settings. At high fluences (low gain) the Landau fluctuations are low and the larger jitter is minimized by large CFD settings.

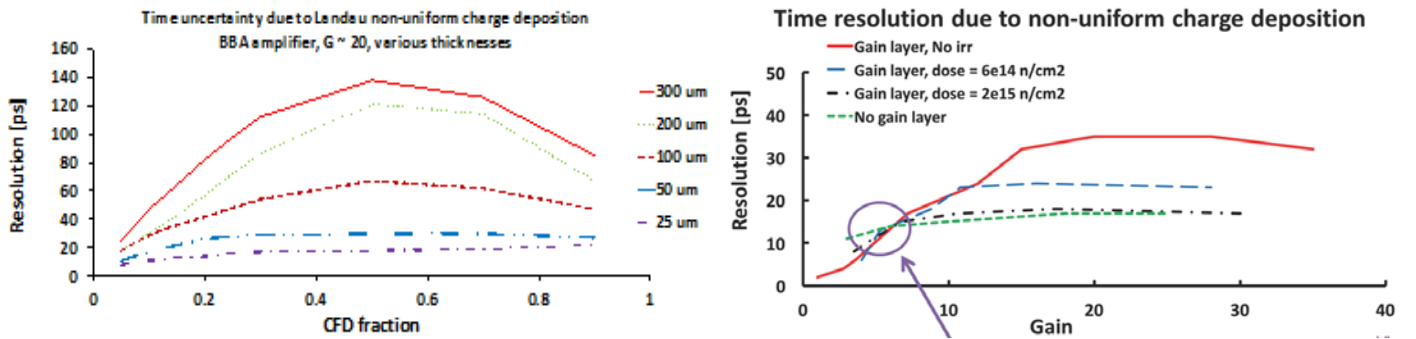


Fig. 13: WF2 prediction of the contribution to the time resolution due to initial non-uniform ionization (Landau fluctuations): pre-radiation as a function of CFD fraction for several thicknesses (left), and as a function of gain for CFD = 20% for several fluences, including no-gain sensors (right). The circle indicates that for gain values of  $\sim 5$  the contribution is roughly constant with irradiation.

### 6.7 Bias Reach – “Headroom”

In order to gauge the performance of the LGAD during operations at the HL-LHC we consider in the following two scenarios for biasing the sensors. One is to bias them at the maximum voltage, just before the current becomes excessive or the resolution deteriorates visibly, which we called the “breakdown voltage”  $V_{\text{BD}}$ . The

other voltage is at least 5% lower than  $V_{BD}$  to assure the stable operation of the LGAD, including minimizing the risk of sensor damage and spurious noise/micro discharges, which we call the “headroom voltage”  $V_{HR}$ . In Fig. 14 and Table 1 the time resolution and the corresponding optimal CFD fraction are shown for both scenarios at the different fluence stages. While for un-irradiated sensors both bias settings are below 300 V, they increase for fluences  $\geq 6e14$  n/cm<sup>2</sup> to 500 V or more (Fig. 14 (left side)). The voltage headroom is 30 V initially and increases to 100 V for fluences above  $1e15$  n/cm<sup>2</sup>. This is important since the optimal operating voltage is well known at the beginning of the experiment, while there will be a certain amount of uncertainty later after large fluences as to how to bias the sensors. The optimal CFD is constant at a low value  $< 20\%$  up to  $1e15$  n/cm<sup>2</sup>, with a sharp increase above that number (Fig. 14 (center)). The time resolution increases with fluence from 20 ps pre-radiation to 50 ps after the highest fluence with small ( $\approx 2 - 4$  ps) increase when changing from  $V_{HR}$  to  $V_{BD}$ . It should be noted that when applying a fixed 20% CFD threshold, the time resolution increases significantly from the value achieved with an optimized CFD threshold only at the highest fluence points (Fig. 14 (right)).

Table 1. Fluence dependence of bias voltages at breakdown ( $V_{BD}$ ) and with headroom ( $V_{HR}$ ) and of the corresponding gain, timing resolution, the CFD fraction (CFD %) and headroom.

Temp.	Fluence [n/cm <sup>2</sup> ]	VBD [V]	Charge [ke]	Gain	Resolution at VBD [ps]	CFD% at VBD	VHR [V]	Charge [ke]	Gain	Resolution at VHR [ps]	CFD% at VHR	Headroom [V]	Headroom [%]
-20C	0	300	251	78.6	20	11	270	124	38.8	22	13	30	10%
-20C	1.E+14	360	133	41.7	25	11	320	70	29.7	26.5	11	40	11%
-20C	3.E+14	600	128	40.1	31	13	550	78	24.4	29	14	50	8%
-20C	6.E+14	650	102	35.5	26.5	10	600	49	17.0	31	10	50	8%
-20C	1.E+15	700	39	13.9	33	16	600	16	5.7	37	28	100	14%
-20C	3.E+15	730	13	5.7	41.5	36	600	4.4	1.9	49	55	130	18%
-20C	6.E+15	600	4.4	2.7	51.5	58	500	3.8	2.4	50	72	100	17%
-30C	6.E+15	600	4.4	2.7	48	65	500	3.7	2.3	46	60	100	17%

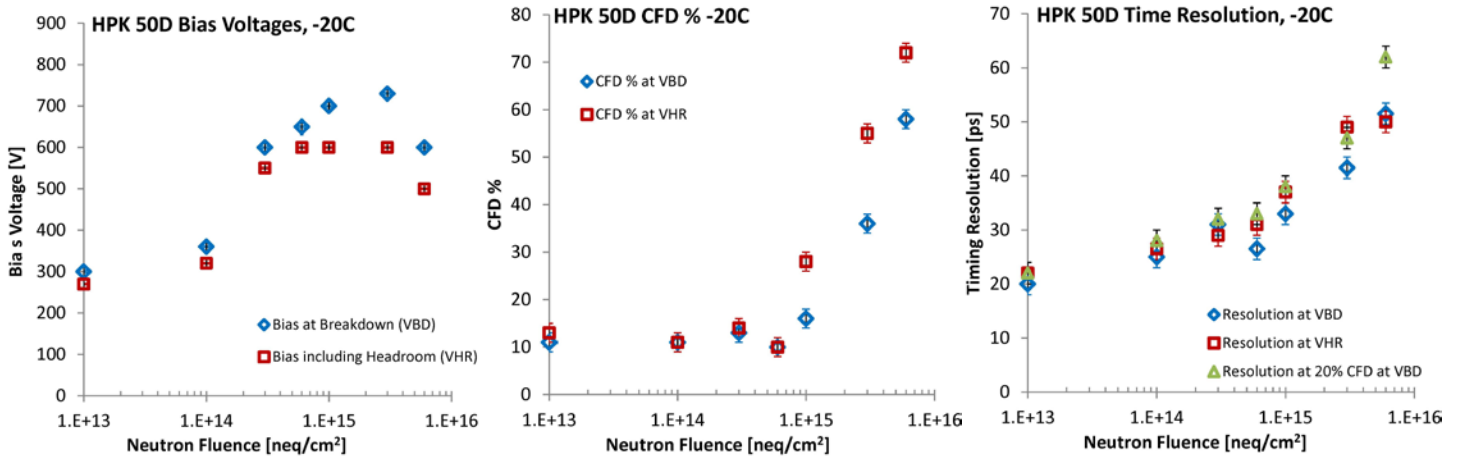


Fig. 14: Fluence dependence of the operating voltages  $V_{BD}$  and  $V_{HR}$  (left), the CFD fractions for best timing resolution at those two bias voltages (center) and the timing resolution for the two bias voltages using those optimized CFD fractions and for a constant CFD fraction of 20% at  $V_{BD}$  (right). (The pre-radiation point is shown at a fluence of  $1e13$ ).

## 7 COMPARISON WITH WF2 SIMULATION

In this section, the capability of the simulation program WF2 to reproduce the key features shown above is explored. Figure 15 shows the comparison between data and WF2 of the pulse shape at representative fluences in absolute values (left side) and normalized (right side). Both the decrease of pulse height, the rise time and the reduction of the tail with fluence are well modelled.

Comparison between data and WF2 predictions of the signal slope ( $dV/dt$ ) vs. gain, the gain vs bias and the rise time vs. gain are shown in Fig. 16. In these variables too there is a good agreement between data and WF2 simulation both in absolute values and in the functional trends as a function of gain and bias. These comparisons are therefore important as they confirm our capability of modelling the dynamic mechanisms of gain including the interplay between gain layer and bulk multiplication, and the effects of radiation damage in UFSD sensors.

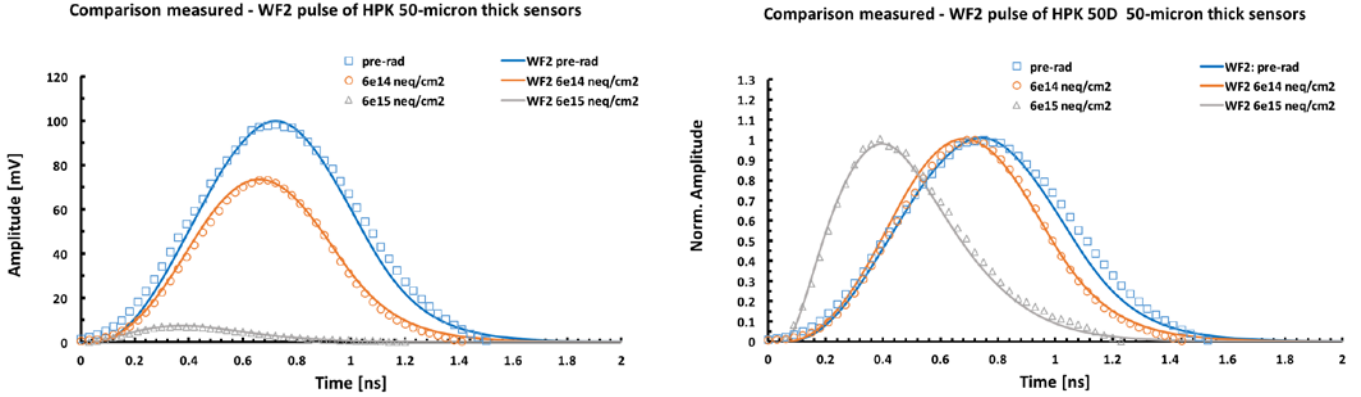


Fig. 15: Data and WF2 prediction of the average pulse shapes for three fluences showing the reduction in gain (left); normalised pulse shapes, showing the decrease in rise time and width of the pulse (right).

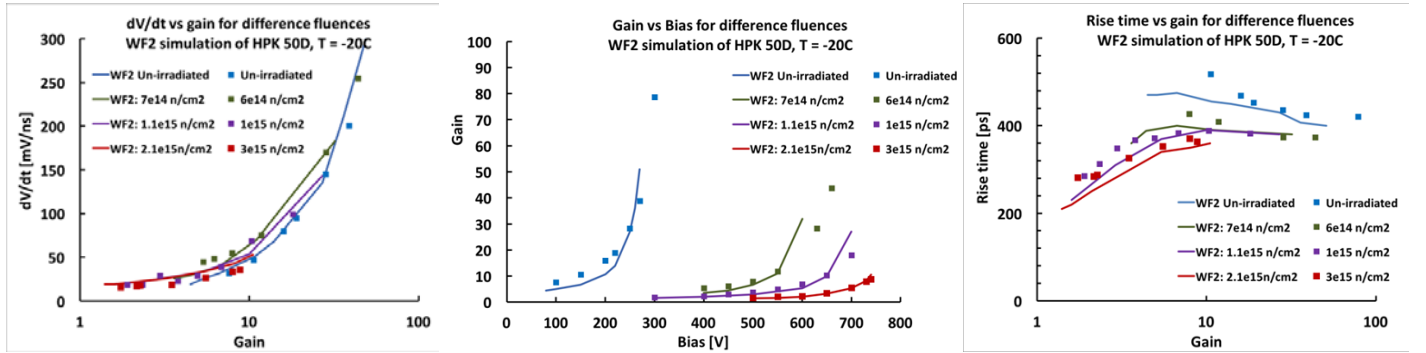


Fig. 16: Comparison of Data and WF2 predictions of the slope  $dV/dt$  vs. gain (left), the gain vs bias (middle) and the rise time vs. gain (right).

## 8 CONCLUSIONS

We have performed a neutron radiation campaign on 50  $\mu\text{m}$  thick UFSD produced by HPK up to a fluence of  $6\text{e}15 \text{ n/cm}^2$ . The sensors were operated at  $-20\text{C}$  and  $-30\text{C}$  to measure as a function of bias voltage the leakage current, gain, timing resolution and pulse shapes. We find

- The bias voltage at breakdown increases from 300 V pre-radiation to 750 V at the highest fluence.
- The gain at the breakdown voltage decreases from 80 pre-radiation to 7 at the highest fluence.
- After dividing by the gain, the fluence dependence of the leakage current agrees fairly well with the expectation for no-gain sensors
- The operating bias, the optimized CFD fraction, the rise time and the timing resolution show a marked change at a fluence of  $1\text{e}15$ . This can be explained by the fact that the multiplication moves from the gain layer to the bulk which leads to a lower gain.
- For a CFD fraction optimised for each fluence and bias, the time resolution increased from 20 ps pre-radiation to 40 ps after  $1\text{e}15 \text{ n/cm}^2$  to 50 ps after  $6\text{e}15 \text{ n/cm}^2$ . The optimized CFD fraction stays constant at 10% to 15% from pre-radiation up to  $1\text{e}15 \text{ n/cm}^2$ , and then increases to  $> 60\%$ .
- Reducing the temperature from  $-20\text{C}$  to  $-30\text{C}$  improves the timing resolution by 10% at large fluences where the gain is reduced to below 3.

- Even though the gain for large fluences is low, the change in the pulse shape, especially the rise time, as a function of fluence is responsible for the good time resolution after large fluences.
- The “headroom” between the breakdown voltage and an operating condition at lower bias causes a reduced timing resolution of a few ps.
- A comparison of results of the measurements with those from the simulation package Weightfield 2 show very good agreement.

## 9 ACKNOWLEDGEMENTS

We acknowledge the expert contributions of the SCIPP technical staff and the HPK manufacturing team. Part of this work has been performed within the framework of the CERN RD50 Collaboration.

The work was supported by the United States Department of Energy, grant DE-FG02-04ER41286. Part of this work has been financed by the European Union’s Horizon 2020 Research and Innovation funding program, under Grant Agreement no. 654168 (AIDA-2020) and Grant Agreement no. 669529 (ERC UFSD669529), and by the Italian Ministero degli Affari Esteri and INFN Gruppo V.

## 10 REFERENCES

- [1] H.F.-W. Sadrozinski, Abraham Seiden, Nicolò Cartiglia, “4-Dimensional Tracking with Ultra-Fast Silicon Detectors”, arxiv 1704.08666.
- [2] G. Pellegrini, et al., “Technology developments and first measurements of Low Gain Avalanche Detectors (LGAD) for high energy physics applications”, Nucl. Instrum. Meth. A765 (2014) 24.
- [3] H.F.-W. Sadrozinski, et al., “Ultra-fast silicon detectors”, Nucl. Instrum. Meth. A831 (2016) 18.
- [4] M. Carulla et al., “First 50  $\mu\text{m}$  thick LGAD fabrication at CNM”, 28th RD50 Workshop, Torino, June 7th 2016,  
<https://agenda.infn.it/getFile.py/access?contribId=20&sessionId=8&resId=0&materialId=slides&confId=11109>.
- [5] RD50 collaboration, <http://rd50.web.cern.ch/rd50/>.
- [6] N. Cartiglia et al., “Beam test results of a 16 ps timing system based on ultra-fast silicon detectors”, Nucl. Instrum. Meth. A850, (2017), 83–88.
- [7] N. Cartiglia et al, “Performance of Ultra-Fast Silicon Detectors”, JINST 9 (2014) C02001.
- [8] N. Cartiglia, “Design optimization of ultra-fast silicon detectors”, Nucl. Instrum. Meth. A796 (2015) 141-148.
- [9] F. Cenna, et al., “Weightfield2: A fast simulator for silicon and diamond solid state detector”, Nucl. Instrum. Meth. A796 (2015) 149; <http://personalpages.to.infn.it/~cartigli/Weightfield2/Main.html>.
- [10] HL-LHC, <http://dx.doi.org/10.5170/CERN-2015-005>.
- [11] L. Gray, “4D Trackers”, at “Connecting the dots”, Paris 2017,  
[https://indico.cern.ch/event/577003/contributions/2476434/attachments/1422143/2180715/20170306\\_LiNdseyGray\\_CDTWIT.pdf](https://indico.cern.ch/event/577003/contributions/2476434/attachments/1422143/2180715/20170306_LiNdseyGray_CDTWIT.pdf).
- [12] G. Kramberger et al.: “Radiation hardness of thin LGAD detectors”, TREDI 2017,  
<https://indico.cern.ch/event/587631/contributions/2471705/attachments/1414923/2165831/RadiationHardnessOfThinLGAD.pdf>.
- [13] H. F.-W. Sadrozinski et al, Timing measurements on UFSD , TREDI 2017,  
<https://indico.cern.ch/event/587631/contributions/2471694/attachments/1415772/2167581/Trento.pptx>.
- [14] J. Lange et al “ Gain and time resolution of 45  $\mu\text{m}$  thin LGAD before and after irradiation up to a fluence of  $10^{15}$  neq/cm<sup>2</sup>”, arXiv:1703.09004.
- [15] G. Kramberger et al., “Radiation effects in Low Gain Avalanche Detectors after hadron irradiations”, JINST 10 P07006, 2015.
- [16] Z. Luce, UCSC Senior Thesis 2017,  
<https://drive.google.com/drive/folders/0ByskYealR9x7bFY1ZS1pZW9SRWs>.
- [17] S. Meroli et al, “Energy loss measurement for charged particles in very thin silicon layers”, JINST 6 (2011) P06013.

- [18] C. Labitan, UCSC Senior Thesis 2017,  
<https://drive.google.com/drive/folders/0ByskYealR9x7bFY1ZS1pZW9SRWs>.
- [19] L. Snoj, G. ˇZerovnik and A. Trkov, Computational analysis of irradiation facilities at the JSI TRIGA reactor, *Appl. Radiat. Isot.* 70 (2012) 483.
- [20] Y Zhao, UCSC Senior Thesis 2017,  
<https://drive.google.com/drive/folders/0ByskYealR9x7bFY1ZS1pZW9SRWs>.